DOI: 10.1002/ejic.201100065

Gallium Pnictides of the Alkaline Earth Metals, Synthesized by Means of the Flux Method: Crystal Structures and Properties of $CaGa_2Pn_2$, $SrGa_2As_2$, $Ba_2Ga_5As_5$, and $Ba_4Ga_5Pn_8$ (*Pn* = P or As)

Hua He,[a] Ryan Stearrett,[b] Edmund R. Nowak,[b] and Svilen Bobev*[a]

Dedicated to Professor John D. Corbett on the occasion of his 85th birthday

Keywords: Alkaline earth metals / Gallium / Pnictides / Solid-state structures / Density functional calculations

The focus of this paper is on the structural characterization of the new Zintl phases $CaGa_2P_2$, $CaGa_2As_2$, $SrGa_2As_2$, and $Ba_2Ga_5As_5$, and the solid solution $(Ba_{0.85(1)}Sr_{0.15})_2Ga_5As_5$, all of which were synthesized from molten metal fluxes. $CaGa_2P_2$, $CaGa_2As_2$, and $SrGa_2As_2$ have layered structures with polyanionic layers made of ethane-like Ga_2P_6 and Ga_2As_6 motifs fused through common edges; the polyanionic substructure in $Ba_2Ga_5As_5$ consists of condensed Ga_2As_6 units and $GaAs_4$ tetrahedra. $Ba_4Ga_5P_8$ and $Ba_4Ga_5As_8$, another pair of new compounds with channel-like 3D structures, were also synthesized from metal fluxes, and their structures were established from single-crystal X-ray and synchrotron powder diffraction. They are based on GaP_4 and $GaAs_4$ tetrahedra, with parts of their structures being heavily disordered. The electronic structures computed with the linear muffin-tin orbital (LMTO) method are discussed as well, alongside the thermopower and the electrical conductivity, measured on single crystals of $Ba_2Ga_5As_5$ and the solid solution $(Ba_{0.85(1)}Sr_{0.15})_2$ Ga_5As_5. They demonstrate that such an approach would be an effective way to fine-tune the transport properties.

Introduction

Zintl phases are typically defined as saltlike compounds, formed between the electropositive metals from groups 1 and 2, and the early p-block elements.[1] The chemical bonding in this class of intermetallic phases is best understood following the Zintl–Klemm formalism,[2] which assumes that the alkali and alkaline earth (or even rare earth) metals donate their valence electrons to the more electronegative metalloid elements; they in turn use these electrons to form covalent bonds to attain closed-shell configurations. As poor metals or small band-gap semiconductors by definition,[3] Zintl phases offer a balance of charge and heat-transport properties that is desirable for thermoelectric development (recall that the thermoelectric figure of merit is $ZT = \sigma\alpha^2T/\kappa$,[4] in which σ is the electrical conductivity, α is the Seebeck coefficient, and κ is the thermal conductivity). Indeed, in recent years, several types of Zintl compounds have received recognition as candidate thermoelectric materials.[5] Examples include but are not limited to $Yb_{14}MnSb_{11}$,[6] $Ca_xYb_{1-x}Zn_2Sb_2$,[7] $Yb_5Al_2Sb_6$,[8] $Eu(Cd_{1-x}Zn_x)_2Sb_2$,[9] and $YbCd_{2-x}Zn_xSb_2$.[10]

Motivated by the discoveries of high ZT among such compounds,[6–10] our research group has been very active in this field. Past efforts have been focused on the search for new thermoelectric materials in the ternary systems *A*–*M*–*Pn* (*A* = Ca, Sr, Ba, Eu, Yb; *M* = Zn, Cd; *Pn* = P, As, Sb, Bi), and we have already reported a number of new compounds, such as Ca_2CdSb_2 and Yb_2CdSb_2,[11] Na_2ACdSb_2 and K_2ACdSb_2,[12] $Eu_{11}Zn_6Pn_{12}$ and $Eu_{11}Cd_6Sb_{12}$,[13] $Ba_{11}Cd_8Bi_{14}$,[14] $A_9Zn_{4+x}Pn_9$ and $A_9Cd_{4+x}Pn_9$,[15] $Ba_3Cd_2Sb_4$,[16] and $Ba_2Cd_2Pn_3$.[17] The synthesis of most of these materials has been facilitated by the metal-flux method,[18] which, unlike the traditional solid-state route, allows the reactants to dissolve in a "solvent" and thereby achieve higher diffusion rates at lower temperatures.[19] Another advantage of the application of a metal flux, which has already been demonstrated on many occasions, is that it makes it possible to avoid the thermodynamic traps of stable binary or ternary compounds, thus increasing the chances for obtaining other competing phases or even metastable phases.[19,20]

By drawing on the previous successful research on pnictides made from In, Zn, Cd, Sn, and Pb as molten-metal fluxes, we also undertook a systematic exploration in the

[a] Department of Chemistry and Biochemistry,
University of Delaware,
Newark, Delaware 19716, USA
E-mail: bobev@udel.edu
[b] Department of Physics and Astronomy,
University of Delaware,
Newark, Delaware 19716, USA

Supporting information for this article is available on the WWW under http://dx.doi.org/10.1002/ejic.201100065.

ternary *A*–Ga–*Pn* systems. Here, the natural choice of a flux would be gallium itself (m.p. 29.8 °C).[21] This approach proved fruitful and readily yielded two new families of antimonides: $A_7Ga_2Sb_6$[22] and $A_7Ga_8Sb_8$.[23] The following studies of the *A*–Ga–P and *A*–Ga–As phase space were also successful from the very beginning: Zintl phases $BaGa_2P_2$ and $BaGa_2As_2$ were recently identified and reported by our group.[24] Other laboratories have utilized the same method to obtain $BaGa_2Sb_2$,[25] $EuGa_2Pn_2$,[26] and $Ba_3Ga_4Sb_5$.[27]

With this paper, we describe more results from the ongoing synthetic and structural studies on new gallium phosphides and arsenides with Ca, Sr, and Ba. Herein we present the layered structures of new Zintl phases $CaGa_2P_2$, $CaGa_2As_2$, $SrGa_2As_2$, $Ba_2Ga_5As_5$, and the solid solution $(Ba_{0.85(1)}Sr_{0.15})_2Ga_5As_5$, which have been accurately established by single-crystal X-ray diffraction. We also detail the combined single-crystal and synchrotron powder diffraction studies, which were used for pinning down the 3D structures of $Ba_4Ga_5P_8$ and $Ba_4Ga_5As_8$ – two convoluted structures that are plagued by extensive Ga disorder. Individual structure and bonding characteristics are discussed and compared, alongside the electronic band structure calculations. Presented as well are the temperature dependences of the Seebeck coefficient and the electrical resistivity, measured on single crystals and cold-pressed pellets.

Results and Discussion

Structure Description

A summary of the single-crystal X-ray diffraction studies of $CaGa_2P_2$, $CaGa_2As_2$, $SrGa_2As_2$, and $Ba_2Ga_5As_5$ is given in Tables 1 and 2; the details for the heavily disordered $Ba_4Ga_5P_8$ and $Ba_4Ga_5As_8$ phases are presented in the Supporting Information. $CaGa_2P_2$, $CaGa_2As_2$, and $SrGa_2As_2$ are formally isoelectronic, but they do not crystallize with the same structures, although common structural motifs are present in all three. $Ba_2Ga_5As_5$ is isoelectronic and isostructural with the recently reported $Ba_2In_5P_5$.[28] Schematic representations of the structures of these compounds are shown in Figures 1, 2, 3; selected structure refinement parameters and relevant interatomic distances are tabulated in Tables 3, 4, 5, and 6. Short descriptions of each structure follow.

$CaGa_2P_2$ is isostructural to $EuIn_2P_2$[29] and crystallizes with the hexagonal space group $P6_3/mmc$ (Pearson symbol *hP*10). Other known compounds that crystallize with the same structure type include $EuIn_2As_2$,[30] $CaIn_2P_2$, and $SrIn_2P_2$.[31] This arrangement features $[Ga_2Pn_2]^{2-}$ or $[In_2Pn_2]^{2-}$ double layers, which are stacked along the direction of the *c* axis (Figure 1). The divalent Ca^{2+} and Sr^{2+} cations fill the octahedral cavities that are created between neighboring layers. The hexagonal structure is described by three crystallographically unique sites in the asymmetric unit, which are occupied by the alkaline earth metal (2*a*), the triel (4*f*), and the pnictogen (4*f*), respectively (Table 3). Since this structure type has been previously discussed,[29–31] we will only point out several important features, mainly in comparison with the structure of $CaGa_2As_2$, which is similar but not identical.

Table 1. Selected crystallographic data for $CaGa_2P_2$ and $CaGa_2As_2$.

	$CaGa_2P_2$	$CaGa_2As_2$
M_r	241.46	329.36
Space group	$P6_3/mmc$ (no. 194)	$R\bar{3}m$ (no. 166)
a [Å]	3.8289(7)	3.9906(4)
c [°]	16.393(4)	24.820(4)
V [Å^3]	208.14(8)	342.31(7)
λ (Mo-K_α) [Å]	0.71073	
Z	2	3
T [K]	200(2)	
$\rho_{calcd.}$ [g cm^{-3}]	3.853	4.793
μ [mm^{-1}]	14.712	27.107
GoF on F^2	1.262	1.212
Final R_1 [$I > 2\sigma(I)$][a]	0.0129	0.0178
Final wR_2 [$I > 2\sigma(I)$])[b]	0.0319	0.0434

[a] $R_1 = \Sigma||F_o| - |F_c||/\Sigma|F_o|$. [b] $wR_2 = \{\Sigma[w(F_o^2 - F_c^2)^2]/\Sigma[w(F_o^2)^2]\}^{1/2}$.

Table 2. Selected crystallographic data for $SrGa_2As_2$ and $Ba_2Ga_5As_5$.

	$SrGa_2As_2$	$Ba_2Ga_5As_5$
M_r	376.9	997.73
Space group	$P2/m$ (no. 10)	$Pnma$ (no. 62)
a [Å]	9.5905(15)	16.729(4)
b [Å]	4.0474(6)	4.1042(9)
c [Å]	12.525(2)	17.214(4)
β [°]	95.699(2)	
V [Å^3]	483.77(13)	1181.9(5)
λ (Mo-K_α) [Å]	0.7107	
Z	4	
T [K]	200(2)	
$\rho_{calcd.}$ [g cm^{-3}]	5.175	5.607
μ [mm^{-1}]	35.421	31.523
GoF on F^2	0.992	1.044
Final R_1 [$I > 2\sigma(I)$][a]	0.0303	0.0274
Final wR_2 [$I > 2\sigma(I)$])[b]	0.0582	0.0607

[a] $R_1 = \Sigma||F_o| - |F_c||/\Sigma|F_o|$. [b] $wR_2 = \{\Sigma[w(F_o^2 - F_c^2)^2]/\Sigma[w(F_o^2)^2]\}^{1/2}$.

$CaGa_2As_2$ crystallizes with a new structure type with the rhombohedral space group $R\bar{3}m$ (no. 166, Pearson symbol *hR*15). There are three independent atomic sites in the asymmetric unit Ca (3*a*), Ga (6*c*), and As (6*c*). The structure can also be rationalized as an array of polyanionic $[Ga_2As_2]^{2-}$ layers that are separated by layers of Ca^{2+} cations (Figure 1). The $[Ga_2As_2]^{2-}$ layers have very similar topology to the $[Ga_2P_2]^{2-}$ layers, except that the former are made up of condensed ethane-like As_3Ga–$GaAs_3$ motifs in staggered conformation, whereas in $CaGa_2P_2$, the P_3Ga–GaP_3 moieties adopt an eclipsed conformation. The stacking sequences of the slabs are different too: triple *ABCABC* in the rhombohedral $CaGa_2As_2$ compared to *ABAB* in the hexagonal $CaGa_2P_2$. One may speculate that the eclipsed conformation seen for Ga_2P_6 would be unfit for the bigger As atoms, thereby causing the twisting around the Ga–Ga bond and the staggered conformation in Ga_2As_6. However, closer examination reveals that the P–P distance in $CaGa_2P_2$ is 4.427 Å, two-and-a-half times larger than the van der Waals radius of As (1.85 Å).[32] In addition, Ga_2Sb_6 eth-

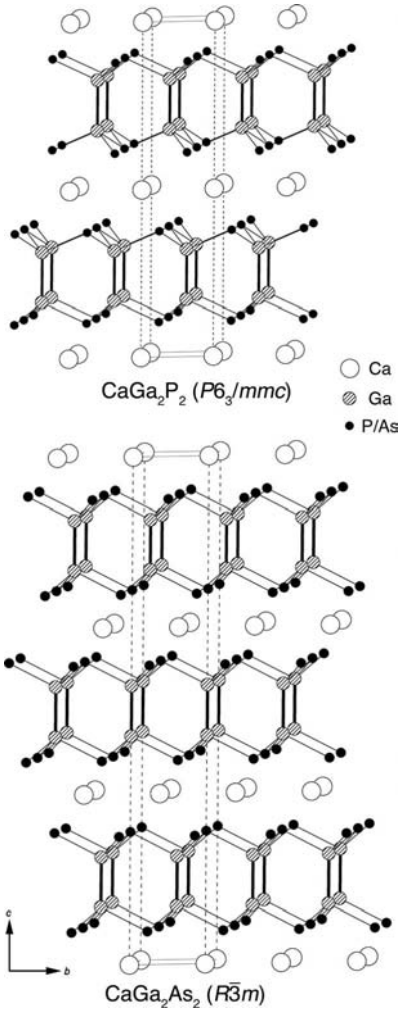

Figure 1. Schematic representations of the structures of $CaGa_2P_2$ (top) and $CaGa_2As_2$ (bottom). P and As atoms are shown as black dots, and Ca atoms are drawn as open circles, respectively. The Ga atoms are shown as striped circles and the Ga_2 dimers are highlighted. The unit cells are outlined.

Table 3. Atomic coordinates and equivalent isotropic displacement parameters (U_{eq})[a] for $CaGa_2P_2$ and $CaGa_2As_2$.

Atom	Site	x	y	z	U_{eq} [Å^2]
		$CaGa_2P_2$			
Ca	2*a*	0	0	0	0.009(1)
Ga	4*f*	$^1/_3$	$^2/_3$	0.1754(1)	0.009(1)
P	4*f*	$^1/_3$	$^2/_3$	0.6150(1)	0.008(1)
		$CaGa_2As_2$			
Ca	3*a*	0	0	0	0.011(1)
Ga	6*c*	0	0	0.4509(1)	0.011(1)
As	6*c*	0	0	0.2561(1)	0.008(1)

[a] U_{eq} is defined as $^1/_3$ of the trace of the orthogonalized U_{ij} tensor.

ane-like motifs are also found in an eclipsed conformation (e.g., in $Na_2Ga_3Sb_3$[33] and $Ba_3Ga_4Sb_5$[27]). Thus, the geometry of Ga_2Pn_6 is most likely not governed by the different sizes of the pnictogens; instead it should be attributed to their electronegativities,[34] which cause variations in the cation–anion interactions. A testament to this line of thinking is the difference between the Ca–P and Ca–As contacts (0.092 Å; Table 4), which is smaller than the difference between the radii of As (r_{As} = 1.21 Å) and P (r_P = 1.10 Å).[34] As a result of the less ionic Ca–As interactions (i.e., more covalent Ca–As), the $[Ga_2As_2]^{2-}$ and Ca^{2+} slabs in $CaGa_2As_2$ pack more tightly than the respective layers in $CaGa_2P_2$. Similar examples in which cation–anion interactions are linked to subtle structural changes have recently been discussed for Ca_2CdSb_2 and Yb_2CdSb_2,[11] $Sr_{21}Cd_4Sb_{18}$ and $Ba_{21}Cd_4Sb_{18}$,[35] as well as $EuIn_2P_2$[29] and $BaIn_2P_2$.[31]

Table 4. Important interatomic distances [Å] for $CaGa_2P_2$ and $CaGa_2As_2$.

$CaGa_2P_2$			$CaGa_2As_2$		
Atom pair		Distance	Atom pair		Distance
Ga–Ga		2.4444(10)	Ga–Ga		2.4390(16)
Ga–P	×3	2.4227(6)	Ga–As	×3	2.5121(5)
Ca–P	×6	2.9051(8)	Ca–As	×6	2.9967(5)

In both structures, the direction of the Ga–Ga bond coincides with the crystallographic *c* axis, with bond lengths that are virtually the same: 2.4390(16) Å in $CaGa_2As_2$ and 2.4444(10) Å in $CaGa_2P_2$ (Table 4).[36] Such distance is on par with the sum of the Pauling's covalent radius (r_{Ga} = 1.246 Å),[34] thereby indicating the presence of strong covalent Ga–Ga bonding. Within the Ga_2As_6 and Ga_2P_6 motifs, the six Ga–As and Ga–P bonds are symmetry-equivalent, and the corresponding distances [$d_{Ga–As}$ = 2.5121(5) Å and $d_{Ga–P}$ = 2.4227(6) Å] compare well with the sums of the respective covalent radii.[34] These values match very well those reported for other compounds with similar bonding patterns, such as $EuGa_2As_2$,[26] $BaGa_2P_2$, and $BaGa_2As_2$,[24] and the Ga–As distances in $SrGa_2As_2$ and $Ba_2Ga_5As_5$ (Table 6). Taking these comparisons into account and emphasizing the covalency of the Ga–Ga and Ga–*Pn* interactions, the electron count for both compounds can be rationalized in accordance with the Zintl concept[2] as $Ca^{2+}(4b\text{-}Ga^{1-})_2(3b\text{-}Pn^0)_2$. Alternatively, by assigning oxidation numbers for purposes of electron bookkeeping, the charges can be considered to be $Ca^{2+}(Ga^{3+})_2(Pn^{3-})_2(e^-)_2$, in which the extra electrons account for the homoatomic Ga–Ga bond. Band-structure calculations (vide infra) confirm this electron count.

$SrGa_2As_2$ crystallizes with much lower symmetry structure than both $CaGa_2P_2$ and $CaGa_2As_2$. It is isostructural to $EuGa_2Pn_2$[26] (monoclinic space group *P*2/*m*, Pearson symbol *mP*20). There are 11 independent atomic sites in the asymmetric unit: three Sr, four Ga, and four As, all in planes at y = 0 and y = $^1/_2$ (Table 5).

The structure again is based on polyanionic $[Ga_2As_2]^{2-}$ layers, separated by Sr^{2+} cations; however, the topology of the layers is different than that previously discussed (Figure 2). Here again, Ga_2As_6 staggered ethane-like motifs are present, but they are not colinear. Instead, Ga–Ga bond orientations in $SrGa_2As_2$ are different: Ga1–Ga2 and Ga4–Ga4 bonds are almost parallel to each other, whereas the third bond, Ga3–Ga3, is in a nearly perpendicular direc-

Table 5. Atomic coordinates and equivalent isotropic displacement parameters (U_{eq})[a] for $SrGa_2As_2$ and $Ba_2Ga_5As_5$.

Atom	Site	x	y	z	U_{eq} [Å^2]
			$SrGa_2As_2$		
Sr1	2*n*	0.1994(1)	$^1/_2$	0.7770(1)	0.011(1)
Sr2	1*d*	$^1/_2$	0	0	0.009(1)
Sr3	1*c*	0	0	$^1/_2$	0.009(1)
Ga1	2*n*	0.1967(1)	$^1/_2$	0.3245(1)	0.010(1)
Ga2	2*n*	0.3950(1)	$^1/_2$	0.2201(1)	0.009(1)
Ga3	2*m*	0.1081(1)	0	0.0636(1)	0.009(1)
Ga4	2*m*	0.3995(1)	0	0.5539(1)	0.009(1)
As1	2*n*	0.2432(1)	$^1/_2$	0.5246(1)	0.008(1)
As2	2*n*	0.2602(1)	$^1/_2$	0.0340(1)	0.008(1)
As3	2*m*	0.0525(1)	0	0.2578(1)	0.008(1)
As4	2*m*	0.5518(1)	0	0.2457(1)	0.008(1)
			$Ba_2Ga_5As_5$		
Ba1	4*c*	0.0192(1)	$^1/_4$	0.6223(1)	0.012(1)
Ba2	4*c*	0.0419(1)	$^1/_4$	0.1292(1)	0.014(1)
Ga1	4*c*	0.1630(1)	$^1/_4$	0.8110(1)	0.013(1)
Ga2[b]	4*c*	0.1771(1)	$^1/_4$	0.4443(1)	0.011(1)
Ga3	4*c*	0.2922(1)	$^1/_4$	0.1270(1)	0.010(1)
Ga4	4*c*	0.3061(1)	$^1/_4$	0.7763(1)	0.012(1)
Ga5[b]	4*c*	0.3214(1)	$^1/_4$	0.4748(1)	0.012(1)
As1	4*c*	0.1177(1)	$^1/_4$	0.3110(1)	0.011(1)
As2	4*c*	0.2952(1)	$^1/_4$	0.6272(1)	0.010(1)
As3	4*c*	0.3786(1)	$^1/_4$	0.0101(1)	0.011(1)
As4	4*c*	0.3860(1)	$^1/_4$	0.2412(1)	0.011(1)
As5	4*c*	0.5973(1)	$^1/_4$	0.5582(1)	0.011(1)

[a] U_{eq} is defined as $^1/_3$ of the trace of the orthogonalized U_{ij} tensor. [b] Near the center of the Ga2–Ga5 bond, the difference Fourier map showed approximately 12 e$^-$Å^{-3} residual density. It was modeled as a partially occupied Ba site [Ba3: x = 0.2502(4); y = $^1/_4$; z = 0.4426(4); site occupation factor (SOF) = 0.072(2)], which follows the arguments discussed previously for $EuGa_2As_2$.[26] The site-occupation factors of Ga2 and Ga5 (in "conflict" with Ba3) were refined as 0.928(2).

tion. The Ga–Ga and Ga–As distances fall in the range 2.4127(14)–2.486(2) Å and 2.5012(13)–2.5496(13) Å, respectively, and compare very well with those seen in $CaGa_2As_2$ (Table 4) and $EuGa_2As_2$.[26] The three crystallographically independent Sr atoms are all in distorted octahedral arrangements of As atoms with Sr–As contacts that range from 3.0680(10) to 3.2308(13) Å. Thus, just like $CaGa_2P_2$ and $CaGa_2As_2$, $SrGa_2As_2$ should be considered a Zintl phase according to the formulation $Sr^{2+}(4b\text{-}Ga^{1-})_2(3b\text{-}As^0)_2$.

Another interesting observation is that compared to the archetypes $EuGa_2Pn_2$,[26] the structure of $SrGa_2As_2$ appears to be free of Ga disorder. In their report on $EuGa_2Pn_2$, Goforth et al.[26] encountered significant residual density around the midpoint of some Ga–Ga bonds. This electron density was interpreted as a partial substitution of Ga_2 dimers with Eu cations. Such structural disorder is common among Ga-containing (and even some In-containing) pnictides, and has already been documented in several other structures, such as $A_7Ga_2Sb_6$ (A = Eu, Sr, Ba)[22] and $A_7Ga_8Sb_8$ (A = Eu, Sr, Ba) and $Ba_7In_8Sb_8$.[23] The very same disorder is also seen for $Ba_2Ga_5As_5$ (vide infra). Since the magnitude of the "effect" is very small (around 5% of the Ga_2 dimers are replaced by cations), one cannot completely rule out the existence of such substitution in

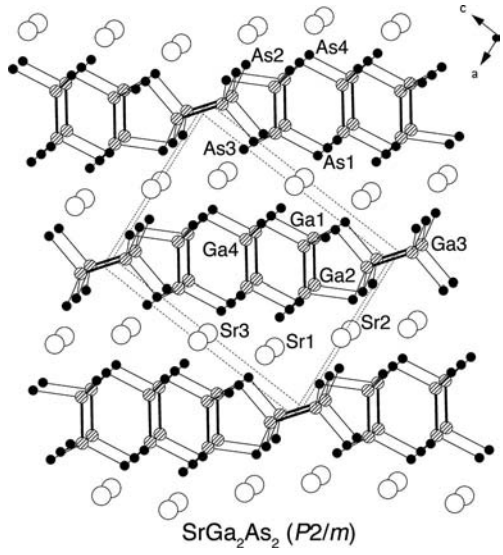

Figure 2. Schematic representation of the structure of $SrGa_2As_2$. Ga atoms are depicted as striped circles, As atoms are shown as black dots, and Ca atoms are drawn as open circles, respectively. The unit cell is outlined.

$SrGa_2As_2$ and even $CaGa_2As_2$. After all, Ca and Sr are much lighter elements than Eu, therefore their X-ray scattering would not cause as significant changes in the Fourier synthesis as Eu would.

$Ba_2Ga_5As_5$ is isostructural to $Ba_2In_5Pn_5$[28] and crystallizes with the orthorhombic space group *Pnma* (no. 62, Pearson symbol *oP*48). It also boasts a layered structure with polyanionic $[Ga_5As_5]^{4-}$ slabs, stacked in an alternating order along the crystallographic a axis, with slabs of Ba^{2+} cations in between (Figure 3). Different from any of the above-described structures, in which the polyanionic layers are made up of only Ga_2Pn_6 units, the $[Ga_5As_5]^{4-}$ substructure in $Ba_2Ga_5As_5$ consists of both condensed Ga_2As_6 ethane-like motifs (staggered, again) and $GaAs_4$ tetrahedra: two Ga_2As_6 fragments form hexagonal channels by sharing common As atoms. These hexagonal "tunnels" are parallel to the crystallographic b axis and are bridged in the direction of the c axis by tetrahedral $[GaAs_2As_{2/2}]$ chains, thereby producing a set of "pentagonal" channels (Figure 3). Similarly complicated bonding patterns have been observed for a few other ternary pnictides (e.g., $Na_2Ga_3Sb_3$[33] and $Ba_3Ga_4Sb_5$[27]). Ga–Ga and Ga–As distances (Table 6) match very well with the corresponding distances, already discussed above. The two different Ba atoms are both surrounded by seven nearest As atoms: the increase of the coordination number on going from Ca^{2+} to Ba^{2+} can be related by the ratio of the radii of the corresponding cations and anions, also known as Pauling's rule.[34] The sevenfold geometry can be described as distorted trigonal prisms with one of their rectangular faces capped by the seventh As neighbor. Notwithstanding the similar coordination polyhedra, the distances between Ba2 and As are generally longer than those between Ba1 and As (Table 3); this difference is closely related to the site preference for the smaller and more electronegative Sr in the

solid solution $(Ba_{0.85(1)}Sr_{0.15})_2Ga_5As_5$ (see Supporting Information). The electron count in this structure can also be approached from the standpoint of the Zintl concept as follows: $(Ba^{2+})_2(4b\text{-}Ga^{1-})_5(4b\text{-}As^{1+})(3b\text{-}As^0)_4$.[37]

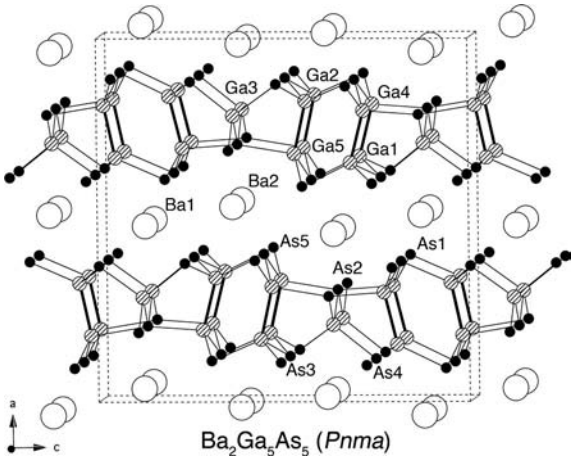

Figure 3. Schematic representation of the structure of $Ba_2Ga_5As_5$. Ga atoms are depicted as striped circles, As atoms are shown as black dots, and Ba atoms are drawn as open circles, respectively. The unit cell is outlined.

Table 6. Important interatomic distances [Å] for $SrGa_2As_2$ and $Ba_2Ga_5As_5$.

$SrGa_2As_2$			$Ba_2Ga_5As_5$		
Atom pair		Distance	Atom pair		Distance
Ga1–Ga2		2.4127(14)	Ga1–Ga4		2.4677(13)
Ga1–As1		2.5012(13)	Ga1–As5		2.5050(13)
Ga1–As3	×2	2.5446(8)	Ga1–As4	×2	2.5155(8)
Ga2–Ga1		2.4127(14)	Ga2–Ga5		2.4701(14)
Ga2–As4	×2	2.5226(8)	Ga2–As1		2.5004(13)
Ga2–As2		2.5496(13)	Ga2–As3	×2	2.5224(8)
Ga3–Ga3		2.486(2)	Ga3–As3		2.4778(12)
Ga3–As3		2.5419(13)	Ga3–As4		2.5150(12)
Ga3–As2	×2	2.5431(8)	Ga3–As2	×2	2.5195(8)
Ga4–Ga4		2.461(2)	Ga4–Ga1		2.4677(13)
Ga4–As4		2.5074(13)	Ga4–As1	×2	2.4894(8)
Ga4–As1	×2	2.5232(8)	Ga4–As2		2.5724(13)
Sr1–As3	×2	3.1489(10)	Ga5–Ga2		2.4701(14)
Sr1–As4	×2	3.1630(10)	Ga5–As5	×2	2.5275(8)
Sr1–As2		3.2143(13)	Ga5–As2		2.6593(14)
Sr1–As1		3.2308(13)	Ba1–As3		3.2756(11)
Sr2–As4	×2	3.0680(10)	Ba1–As1	×2	3.2822(9)
Sr2–As2	×4	3.1239(7)	Ba1–As3	×2	3.2959(9)
Sr3–As1	×4	3.0806(7)	Ba1–As4	×2	3.3036(8)
Sr3–As3	×2	3.1239(10)	Ba2–As5	×2	3.3357(9)
			Ba2–As5		3.3569(12)
			Ba2–As1		3.3756(11)
			Ba2–As2	×2	3.4113(9)
			Ba2–As4		3.4325(11)

Before discussing the 3D-framework structures of $Ba_4Ga_5P_8$ and $Ba_4Ga_5As_8$, which are topologically very different from the above-described $CaGa_2P_2$, $CaGa_2As_2$, and $SrGa_2As_2$, it is useful to consider a unifying theme that bridges and relates the latter to other common types. For instance, $CaGa_2P_2$, $CaGa_2As_2$, and $SrGa_2As_2$ can all be readily derived from a simple close-packed structure, such as TiAs (or its ternary variant, the $AlCr_2C$ type, space group $P6_3/mmc$; Pearson symbol $hP8$).[38] In this structural arrangement, exemplified by $BaCeN_2$[39] in Figure 4, the pnictogen atoms form a double hexagonal close-packed (*hcp*) array, with trigonal prismatic and octahedral holes occupied by Ba and Ce, respectively. Similarly, the $CaGa_2P_2$ structure can be viewed as a double *hcp* array of P^{3-}, which forms the same trigonal prisms and regular octahedra. Here, the octahedral holes are taken up by the Ca^{2+} cations, whereas the trigonal prisms, instead of another alkaline earth or rare earth metal cation, are occupied by Ga_2 dimers, formally $[Ga_2]^{4+}$. From this conjecture, such a substitution of a metal cation for a triel dimer appears to be nothing out of the ordinary, and offers a plausible explanation for the frequency of related structural disorder, encountered in many gallium pnictides.[22–26] Continuing the analogy to $CaGa_2As_2$, one can reason that the bigger As^{3-} anions will allow for more efficient cubic close packing (*ccp*), thus leaving behind only octahedral holes with Ca^{2+} and $[Ga_2]^{4+}$ in them. From such geometric considerations, one can then argue that these two structures will be realized only with the small (light) pnictogens and the small-/medium-sized divalent cations. All attempts to synthesize analogous antimonides, have so far led to layered compounds $A_7Ga_8Sb_8$ (A = Eu, Sr, Ba).[23] The latter can be thought as intergrowth structures of AGa_2Sb_2 ($EuIn_2P_2$ type) and AGaSb (YPtAs type); they indeed are stabilized by larger cations (never Ca^{2+} or Yb^{2+}).

Moving onto the monoclinic $SrGa_2As_2$ structure, one can then suggest that with increasing sizes of the cations, the high symmetry arrangement will become less suitable and new packing modes will result. This is indeed the case. In the $EuGa_2As_2$-type structures, the As^{3-} anions form a very distorted *hcp*-like array to accommodate the bigger Sr^{2+} (or Eu^{2+}) cations. The As atoms lie on corrugated planes, which leads to significant changes in the As_3Ga–$GaAs_3$ motifs; as mentioned earlier, the direction of every fourth Ga–Ga bond is nearly perpendicular to the directions of the adjacent Ga–Ga bonds (Figure 4). For $Ba_2Ga_5As_5$, we may speculate that the very large Ba^{2+} cations cannot be effectively "screened" by the As^{3-} anions in octahedral environments, thereby requiring an increase in the coordination number to CN 7 (Table 6). This is done by alteration of the polyanionic layer, whereby the regular slab of fused Ga_2As_6 octahedra is "cleaved" into dyads, with tetrahedral cavities being created in between them. Every tetrahedral hole is filled with trivalent Ga^{3+}, which accounts for the new stoichiometry $[Ga_5As_5]$.

Last, we will briefly discuss $Ba_4Ga_5P_8$ and $Ba_4Ga_5As_8$. The two compounds crystallize in different space groups—the former with *Ibam*, the latter with *C*2/*c* (for further details, see Supporting Information)—but the two structures are very similar. Regardless of the difference in symmetry, both are extensively disordered in a nearly identical manner. Because of the disorder, which could have been an artefact of poor crystal quality, the routine structural work based on single-crystal X-ray diffraction was complemented by synchrotron powder diffraction. These

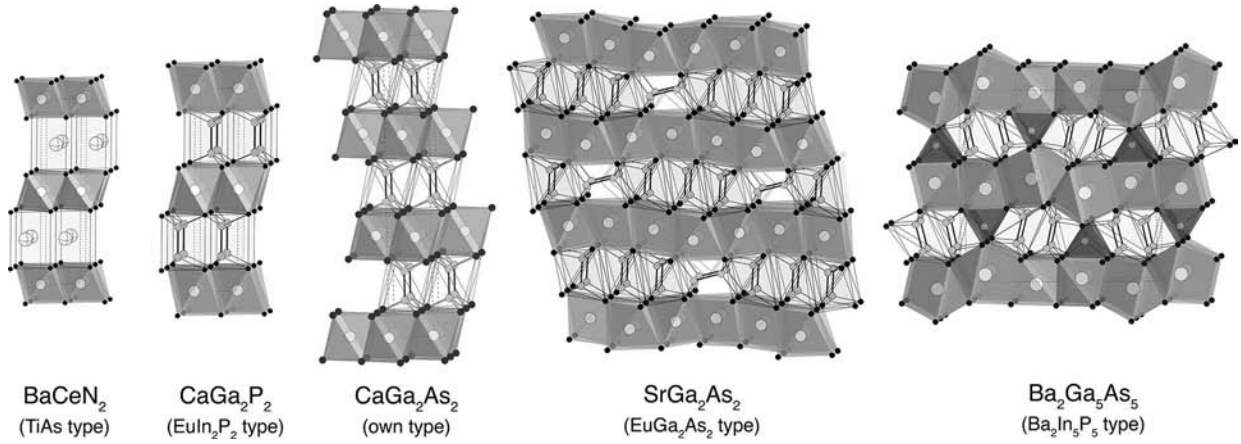

Figure 4. Structural relationship among $CaGa_2P_2$, $CaGa_2As_2$, $SrGa_2As_2$, and $Ba_2Ga_5As_5$. From the point of view of polyhedral packing, all structures appear to be rooted to the double-hexagonal close packing in the TiAs type.

combined efforts, however, led only to the identification of the average structure; the actual atomic structure is likely modulated and could not be unequivocally established as a part of this study. A schematic representation of an idealized ordered structure with a formula $Ba_4Ga_5Pn_8$ is given in Figure 5; structural representations of the refined structures (including the partially occupied sites) are provided in the Supporting Information. Were it free of disorder, $Ba_4Ga_5Pn_8$ could be best viewed as $[Ga_4Pn_4]$ slabs, isosteric with the ubiquitous PbO type, which are interconnected in another direction with isolated $GaPn_4$ tetrahedra. Ba^{2+} cations are located within the resulting "channels" in very distorted polyhedra with CN 7. In Figure 5, for clarity, the $Ba_4Ga_5Pn_8$ formula is broken down to two hypothetical fragments with familiar bonding: (1) Ba_4GaPn_4, which is isotypic with Ba_4SiAs_4,[40] and (2) $GaPn$ with a PbO-like pattern.[41] All Ga–P and Ga–As distances refined from the well-behaved segments of the structure compare very well with the distances in $CaGa_2P_2$, $CaGa_2As_2$, $SrGa_2As_2$, $BaGa_2As_2$, and $BaGa_2P_2$.[24] Interestingly, the structures are devoid of Ba disorder, and all Ba–P and Ba–As distances, including those to partially occupied atoms, are on par with the sum of the corresponding elemental radii.[34]

Another relevant parallel can be drawn between the structure of $Ba_4Ga_5P_8$, in particular, and the recently reported Ba_2ZnPn_2 (K_2SiP_2 type).[42] We succinctly recall that this structure contains chains of edge-shared tetrahedra (e.g., $[ZnPn_{4/2}]$), isosteric with those in the silicon dichalcogenides,[43] surrounded by cations. A good starting point for a discussion here is the observation that in Ba_2ZnPn_2, the chains are formed by *Pn* atoms in a *ccp*-like array, with zinc atoms occupying only $^1/_4$ of the available tetrahedral holes. Expanding on this analogy, one can see that the same *ccp*-like array of *Pn* atoms with $^1/_8$ of the tetrahedral holes filled by Ga will account for isolated $GaPn_4$ tetrahedra (e.g., Ba_4SiAs_4 type), whereas $^1/_2$ filling of the available tetrahedral holes will yield 2D $GaPn$ slabs (PbO type), respectively. Further, since the $Ba_4Ga_5P_8$ and Ba_2ZnPn_2 structures have identical space groups (*Ibam*) with similar unit-cell dimensions, it is intuitive to suggest that the above-mentioned

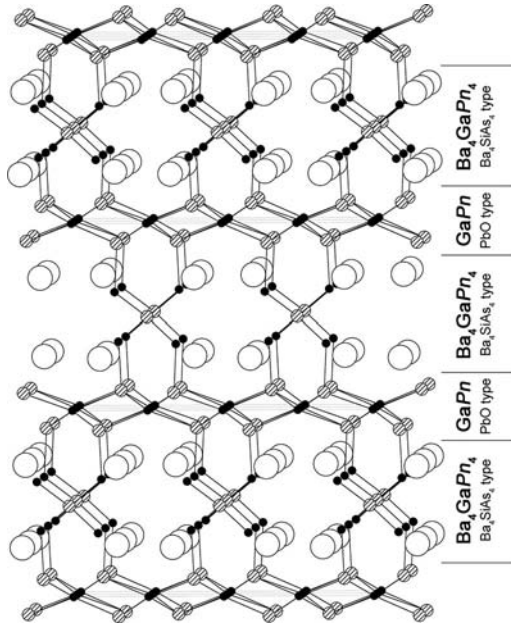

Figure 5. Schematic representation of the idealized structure of $Ba_4Ga_5Pn_8$, made up of Ba_4GaPn_4 (Ba_4SiAs_4 type) and distorted Ga_4Pn_4 (PbO type) slabs. Ga atoms are depicted as striped circles, pnictogen atoms are shown as black dots, and Ba atoms are drawn as open circles, respectively.

structural motifs can "co-crystallize" in the same extended symmetry. Therefore, we can argue that $Ba_4Ga_5P_8$ and $Ba_4Ga_5As_8$ are best explained as intergrowth structures of inherently disordered K_2SiP_2, Ba_4SiAs_4, and PbO-like fragments.[44]

Electronic Structure

The electronic structures were calculated using the tight-binding linear muffin-tin orbital (TB-LMTO) method[45] and using the Stuttgart code.[46] Crystallographic data from the single-crystal structures were used, neglecting the small Sr/Ba–Ga disorder in $SrGa_2As_2$ and $Ba_2Ga_5As_5$. Because

of the extensive disorder, $Ba_4Ga_5Pn_8$ could not be treated. The respective plots of the density of states (DOS) and the crystal orbital Hamilton population (COHP) diagrams are shown in Figures 6 and 7.

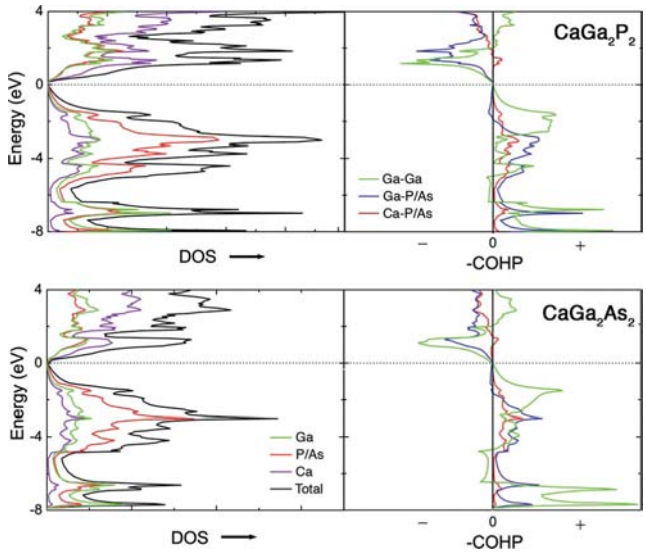

Figure 6. Total and partial DOS and COHP for $CaGa_2P_2$ and $CaGa_2As_2$. The partial DOS and the various COHP curves are indicated on the graphs and color-coded for clarity. Since the "inverted" COHP values are plotted, the positive regions represent the bonding interactions, whereas the negative regions denote the states with antibonding character. E_F (dotted line) is the energy reference at 0 eV.

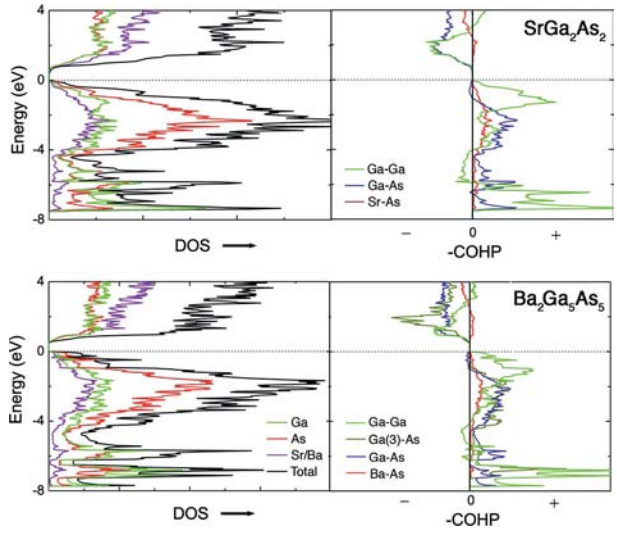

Figure 7. Total and partial DOS and COHP for $SrGa_2As_2$ and $Ba_2Ga_5As_5$. The partial DOS and the various COHP curves are indicated on the graphs and color-coded for clarity. Since the "inverted" COHP values are plotted, the positive regions represent the bonding interactions, whereas the negative regions denote the states with antibonding character. E_F (dotted line) is the energy reference at 0 eV.

As expected from the similar crystal structures, $CaGa_2P_2$ and $CaGa_2As_2$ show similar characteristics in their electronic structures. In both cases, the Ca–*Pn*, Ga–Ga, and Ga–*Pn* bonding is optimized, and the Fermi levels are located in pseudogaps. This is a typical feature of the polar intermetallics in general, and the Zintl phases in particular, thereby confirming the previously discussed electron counting. The states just below the Fermi level, down in energy to approximately –5 eV, are predominately from the Ga and *Pn* valent states (e.g., 3p and 4p). As seen from the COHP diagrams, the Ga–Ga interactions are fully optimized at the Fermi level, thus indicating strong covalent character, which could be deduced from the Ga–Ga distances (vide supra). The Ga–*Pn* interactions in this energy window are nearly optimized and show weak antibonding character just below the Fermi level. The states farther away from the Fermi level, from around –8 to –5 eV are mainly contributed from the p orbitals of the pnictogens and the s orbitals of Ga. Well below the reference point, significant gaps from –8 to –11 eV are noticed for both compounds, below which are the localized s pairs on the triply bonded P or As.

Near the top of the valance band, the contribution from the Ca 3d orbitals to the total DOS is also noticeable, thereby indicating a certain degree of covalency of the Ca–*Pn* interactions. Their COHP curves show that they remain weakly bonding just above the Fermi level, but populating these states would destabilize the system because of the counteracting antibonding Ga–Ga and Ga–*Pn* interactions. Such traits are not without precedents, as similar bonding characteristics have already been observed and studied in $BaGa_2Pn_2$,[24] $BaGa_2Sb_2$,[25] and $Ba_2In_5Pn_5$,[28] among others. From the above, one could predict poor metallic behavior for both $CaGa_2P_2$ and $CaGa_2As_2$, which unfortunately could not be validated experimentally (due to inadequate crystal quality and lack of phase-pure polycrystalline samples).

The DOS and COHP diagrams of $SrGa_2As_2$ are shown in Figure 7. A small band gap (around 0.2 eV) is observed for $SrGa_2As_2$, thereby suggesting that the compound should be an intrinsic semiconductor. However, the substitution of Ga_2 dimers by Sr^{2+}, a disorder that seems to be inherent to the crystal structure (vide supra), may very well change the electronic structure. This will likely give rise to metallic behavior, which has been indeed observed for the isoelectronic and isostructural $EuGa_2Pn_2$ compounds.[26] The states around the Fermi level originate predominately from As and Ga 4p orbitals, with a small admixture of Sr 4d orbitals. The COHP curves show that the Ga–Ga interactions are fully optimized at the Fermi level, whereas the Ga–As interactions exhibit weak antibonding character. The Sr–As interactions, on the contrary, retain their bonding character even slightly above the Fermi level. Similar features in the electronic structure were discussed above for $CaGa_2P_2$ and $CaGa_2As_2$, since they are closely related in structure and share common bonding characteristics.

The electronic structure of $Ba_2Ga_5As_5$ was also calculated for an idealized structure, excluding the Ba–Ga disorder. Since the actual $Ba_{2+x}Ga_{5-2x}As_5$ structure has around 7% of the Ga_2 dimers substituted by Ba, we were unable to model this scenario computationally. Therefore, it is not surprising that there is a discrepancy between the theory

and experiment: the DOS diagram (Figure 7) predicts intrinsic semiconducting behavior with a band gap of around 0.4 eV, comparable with that of the isoelectronic and isostructural $Ba_2In_5As_5$,[28] whereas a metallic-like temperature dependence of the electrical resistivity is experimentally observed for both $Ba_2Ga_5As_5$ and $Ba_2In_5As_5$. The metallicity is obviously due to the small structural disorder (vide infra) and the resulting slight "off-stoichiometry" in both structures (i.e., $Ba_{2+x}Ga_{5-2x}As_5$ and $Ba_{2+x}In_{5-2x}As_5$), which either introduces donor levels in the gap or causes the gap to disappear altogether.

As seen from DOS, the major contribution of the states around Fermi level is from the 4p orbitals of As and Ga, as well as a considerable amount of Ba 5d states. The COHP curves display the averaged interactions between selected atom pairs, for which the COHPs of Ga–As have been grouped into two types based on the different chemical environment of Ga. The interactions between the Ga in the tetrahedral chain (Ga3) and As are nearly optimized at the Fermi level, whereas the interactions between the Ga atoms that form dimers and As display week antibonding character, as we have already noted for $CaGa_2P_2$, $CaGa_2As_2$, and $SrGa_2As_2$. However, due to the extended Ga5–As distances, largely due to the Ga5–As2 contact, which is 2.6593(14) Å (Table 6), the Ga5–As interactions are not as strong as the other Ga–As interactions. This point is better seen from the integrated COHP (–iCOHP) values given in Table 7. From the tabulated data, it is also evident that the Ga5–Ga2 bond is weaker than the Ga1–As4 bond, which explains why the disorder predominantly concerns the former, not the latter.

Table 7. Averaged Ga–As and Ga–Ga distances in $Ba_2Ga_5As_5$, and their corresponding integrated COHP (–iCOHP) values.

	Avg. distance [Å]	–iCOHP
Ga1–As	2.5120	2.40541
Ga2–As	2.5151	2.43721
Ga3–As	2.5080	2.49445
Ga4–As	2.5171	2.28314
Ga5–As	2.5714	2.13012
Ga1–Ga4	2.4677	2.54401
Ga2–Ga5	2.4701	2.51204

The last point with regard to the electronic structure of $Ba_2Ga_5As_5$, which is also relevant to the solid solution $(Ba_{1-x}Sr_x)_2Ga_5As_5$ concerns the atomic orbital populations (AOPs) of the two independent Ba positions. We computed those parameters following the ideas proposed by G. J. Miller,[47] with the objective to understand the preferential mixing of Ba and Sr at the Ba1 site, whereas the Ba2 site-occupation factor showed no statistically significant deviation from full occupancy by Ba (see Supporting Information). We already mentioned that, on average, the Ba1–As distances are shorter than the Ba2–As ones (Table 3), which will favor Ba substitution with the smaller Sr at the Ba1 site, a reasoning that is corroborated by the larger d-orbital population of Ba1 (1.195), compared to that of Ba2 (1.085). From the above, and recalling that the more electronegative atom will stabilize the site with higher "charge," it is clear that the more electronegative Sr[34] will prefer the Ba1 to the Ba2 site. However, since isostructural $Sr_2Ga_5As_5$ or $Sr_2Ga_5P_5$ could not be synthesized, we can suggest that the structure is very cation-sensitive, and that the solubility limit of Sr in it is very low (<20 atom-%). An indirect proof of that conjecture is the fact that Sr–Ga–As reactions yield other phases, and $(Ba_{0.85(1)}Sr_{0.15})_2Ga_5As_5$ was actually obtained from reactions aimed at the 1:1 solid solution.

Physical-Property Measurements

The small crystal size of $CaGa_2P_2$, $CaGa_2As_2$, $SrGa_2As_2$, and $Ba_4Ga_5Pn_8$ impeded the resistivity measurements on single crystals for these samples. Four-probe measurements were only possible for the single crystal of $Ba_2Ga_5As_5$, and the temperature dependence of the resistivity of this compound is shown in Figure 8. The temperature dependence is nearly linear with a positive $d\rho/dT$, which is suggestive of a metallic-like conductivity. The room-temperature value $\rho_{300} = 5.5 \times 10^{-4}\ \Omega\,cm$, is close to the room-temperature resistivities of $EuIn_2As_2$[30] and $Ba_2In_5As_5$.[28] Since the stoichiometric and defect-free $Ba_2Ga_5As_5$[37] is expected to be a semiconductor, the observed metallic behavior most likely originates from the disorder of the structure.

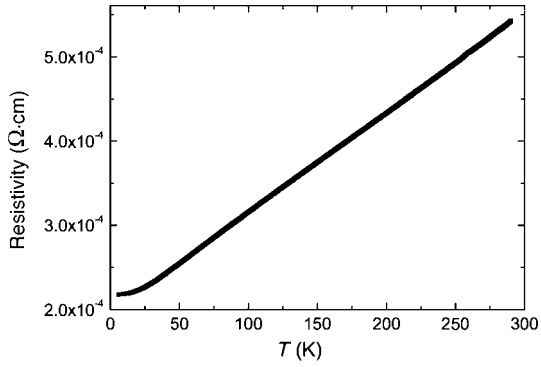

Figure 8. Temperature-dependent resistivity of $Ba_2Ga_5As_5$, measured on a single crystal.

Figure 9 shows the Seebeck coefficients (α) of $Ba_2Ga_5As_5$ and $(Ba_{0.85(1)}Sr_{0.15})_2Ga_5As_5$. Both have positive values in the measured temperature range, thereby suggesting that the predominant charge carriers in these materials are holes (h^+). The Seebeck coefficients increase almost linearly with an increase in temperature. The α value at room temperature for the solid solution $(Ba_{0.85(1)}Sr_{0.15})_2Ga_5As_5$ is slightly higher than the end member $Ba_2Ga_5As_5$, 73 versus 59 $\mu V K^{-1}$. Such difference in the Seebeck coefficients is somewhat surprising given the more covalent nature of the Sr–As interactions compared to Ba–As (vide supra). This experimental conundrum can be explained by an inconspicuous difference in the structural disorder in both structures, which leads to different "off-stoichiometry" in $Ba_{2+x}Ga_{5-2x}$-

As_5 compared to $(Ba,Sr)_{2+x}Ga_{5-2x}As_5$ (the largely different residual peaks, when both structure are refined as fully ordered, are clearly shown in Table S1 in the Supporting Information).

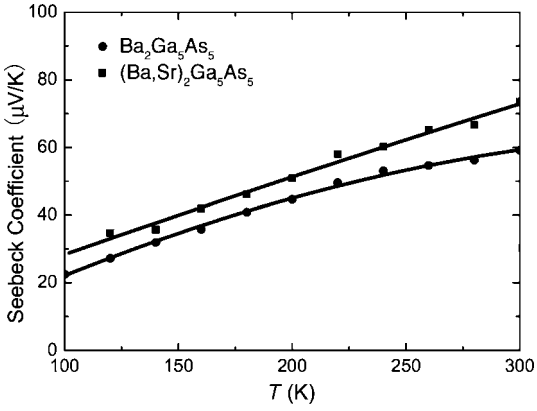

Figure 9. Temperature dependence of Seebeck coefficients (α) of $Ba_2Ga_5As_5$[37] and $(Ba_{0.85(1)}Sr_{0.15})_2Ga_5As_5$.

Conclusion

Six new Zintl compounds were synthesized using Ga as reactive flux. Whereas $CaGa_2P_2$, $SrGa_2As_2$, and $Ba_2Ga_5As_5$ were found to be isostructural to the reported compounds $EuIn_2P_2$,[29] $EuGa_2As_2$,[26] and $Ba_2In_5As_5$,[28] respectively, $CaGa_2As_2$ crystallizes with its own structure type. This new rhombohedral structure features $[Ga_2As_2]^{2-}$ layers with similar topology as the $[Ga_2P_2]^{2-}$ layers in $CaGa_2P_2$. Electronic calculations suggest that $CaGa_2P_2$ and $CaGa_2As_2$ are semimetals, and $SrGa_2As_2$ and $Ba_2Ga_5As_5$ are semiconductors. Resistivity measurement as a function of the temperature on a single crystal of $Ba_2Ga_5As_5$ showed metallic behavior, likely due to a small structural disorder, whereby non-isoelectronic substitution of Ba^{2+} cations for dimeric $[Ga_2]^{4+}$ units occurs. The Seebeck coefficients of $Ba_2Ga_5As_5$ and the solid solution $(Ba_{0.85(1)}Sr_{0.15})_2Ga_5As_5$ indicate tunable transport properties.

Experimental Section

Synthesis: All manipulations involving the alkaline earth metals were performed inside an argon-filled glovebox or under vacuum. The starting materials were elemental Ca, Sr, Ba, Ga, As, and P, purchased from either Alfa Aesar or Aldrich (with stated purity greater than 99.9% metal basis), and were used as received. Millimeter (in rare cases) and submillimeter (typical) size single crystals of the title compounds could be obtained from reactions of the corresponding elements in which an excess amount of Ga was used as a reactive flux. Details on the metal-flux method can be found elsewhere.[18,19] In some instances, in particular the disordered $Ba_4Ga_5P_8$ and $Ba_4Ga_5As_8$, the use of Pb flux was advantageous. Stoichiometric reactions in welded Nb and Ta ampoules were also tried but were found less suitable because the single-crystal quality was inadequate for further studies. In addition, at high temperatures, due to unwanted side reactions, many of the samples were contaminated with Nb–*Pn* or Ta–*Pn* binaries.

The synthetic procedure for $CaGa_2P_2$, $CaGa_2As_2$, and $SrGa_2As_2$ was identical to the optimized reaction scheme used for the crystal growth of $BaGa_2P_2$ and $BaGa_2As_2$ (described in detail in an earlier paper[24]). The alkaline earth metals and P (As) were taken in stoichiometric ratios, whereas Ga was used in fivefold excess amount to serve as a self-flux. Reaction mixtures were heated fast to 1233 K, homogenized for 20 h, and then cooled at a rate of 6 K h^{-1} to 773 K, at which point the molten Ga was decanted. The crystals of $CaGa_2P_2$ had a platelet shape with hexagonal facets; the $CaGa_2As_2$ crystals were flakelike, and the crystals of $SrGa_2As_2$ had the shape of irregular parallelepipeds.

Small amounts of $Ba_2Ga_5As_5$ were first identified as a byproduct of a reaction aimed at producing $BaGa_2As_2$.[24] After the structure was established, the reaction was attempted again with the proper molar ratio (and Ga in fivefold excess amount), however, this reaction did not produce pure-phase $Ba_2Ga_5As_5$ either: another new phase was also present, and it was later identified as $Ba_4Ga_5As_8$. After numerous trials, the optimized heat treatment for $Ba_2Ga_5As_5$ was determined to be: isotherm at 1233 K for 20 h, followed by slow cooling to 1023 K with a rate of 3 K h^{-1}. At this point, the sample was removed and radiatively cooled to room temperature. Finally, the sealed tube was quickly reheated to 773 K (rate 100 K h^{-1}), before the Ga flux was decanted and the reaction product—lots of needle crystals of $Ba_2Ga_5As_5$—was isolated. Similar reactions of Sr, Ga, and As (or P) did not afford isostructural $Sr_2Ga_5As_5$ and $Sr_2Ga_5P_5$ phases, which suggests that the structure is very cation-sensitive.

As mentioned already, $Ba_4Ga_5As_8$ was also initially obtained from a reaction loaded with Ba, Ga, and As in a ratio Ba/Ga/As = 1:10:2, in which again the excess amount of Ga was intended as a flux. The reaction scheme was the same as above, except that the cooling rate was changed to 30 K h^{-1}. Since the structure of $Ba_4Ga_5As_8$ contained extensive disorder, we attempted to anneal the product at 573 K for two weeks, but it proved unsuccessful; the problems persisted. Attempts were also made to synthesize $Ba_4Ga_5As_8$ using Pb flux; however, the crystals from such reactions exhibited the same extent of disorder. Analogous reactions with Ba, Ga, and P afforded the black, panel-shaped crystals of $Ba_4Ga_5P_8$, which crystallizes with a slightly different structure from that of $Ba_4Ga_5As_8$, albeit similarly disordered.

X-ray Powder Diffraction: All powder X-ray diffraction patterns were taken at room temperature with a Rigaku MiniFlex powder diffractometer using filtered Cu-K_α radiation. The data analysis was carried out with the JADE 6.5 software package. The patterns were used to analyze the products from the reactions. Because of the limitations of the in-house powder diffractometer, high-resolution synchrotron powder diffraction data were collected with a beamline 11-BM instrument at the Advanced Photon Source (APS), Argonne National Laboratory. Crystals from the samples were picked under a microscope and ground into fine powder, and then packed in Kapton tubes with inner diameter of 0.8 mm. The data was collected at room temperature using radiation with a wavelength of 0.413984 Å. The scans covered 2θ range from 0.5° to 50°, with data points collected every 0.001° and scan speed of 0.01° s^{-1}. Rietveld refinements were performed on the collected data with the aid of the EXPGUI-GSAS software.[48]

Since the portable Rigaku MiniFlex diffractometer was enclosed and operated in a nitrogen-filled glovebox, the air sensitivity of the title compounds could be checked by comparing the diffraction patterns of the freshly prepared samples and the samples that had

been exposed to air. Based on the gathered results, it was estimated that polycrystalline $CaGa_2P_2$, $CaGa_2As_2$, $SrGa_2As_2$, and $Ba_2Ga_5As_5$ samples are stable in dry air for up to two weeks.

Single-Crystal X-ray Diffraction: Single crystals of the title compounds were chosen in the glovebox, cut to suitable sizes for data collection, and mounted on glass fibers using Paratone-N® oil. Intensity data collections were carried out at 200 K with a Bruker SMART CCD-based diffractometer. Intensity data were collected in four batch runs at different ω and ϕ angles (up to $2\theta_{max} \approx 57°$). The data collections were handled using the SMART software.[49] Data integration was done using SAINTplus,[49] and SADABS[50] was used for semiempirical absorption correction based on equivalent reflections. The structures were solved by direct methods and refined by full-matrix least-squares on F^2 using SHELXL.[51] Refined parameters included the scaling factors, atomic positions, anisotropic displacement parameters, and the site occupancies (where applicable). Details of the structure refinement and crystal data are summarized in Table 1 and Table 2.

Further details on the crystal structure investigation(s) can be obtained from the Fachinformationszentrum Karlsruhe, 76344 Eggenstein-Leopoldshafen, Germany (fax: +49-7247-808-666; E-mail: crysdata@fiz-karlsruhe.de), on quoting the depository number CSD-422525 (for $CaGa_2P_2$); -422526 (for $CaGa_2As_2$); -422527 (for $SrGa_2As_2$); -422528 (for $Ba_2Ga_5As_5$). Several important issues regarding the structural analysis, worthy of a specific mention, are provided below.

Since $Ba_2Ga_5As_5$ showed similar cell parameters to $Ba_2In_5As_5$,[28] the structure was refined with the same space group *Pnma* and using the published coordinates. However, a significant residual density, on the order of 12 $e^-Å^{-3}$, remained in the difference Fourier map after refinements with anisotropic displacement parameters and proper weights. The residual peak was also present in data sets collected for other crystals from different reaction batches. It was located near the center of a distorted octahedron of As atoms; however, this octahedron was not empty, but contained a Ga_2 dimer (i.e., the ethane-like Ga_2As_6 unit discussed in the text). A similar problem has been recently discussed for $EuGa_2As_2$,[26] and following the model from the latter study, the residual density was assigned as a partially occupied Ba site (Ba3). Of course, this model would be physically unrealistic, unless Ga2 and Ga5 that form this dimer are missing whenever Ba3 is present. A follow-up refinement with varied site occupancies of Ba3, Ga2, and Ga5 confirmed that the Ba3 site is around 7% occupied, whereas Ga2 and Ga5 sites are around 93% occupied. The Ba3 atom is at a distorted octahedral coordination with Ba3–As distances in the range of 3.170(7)–3.274(5) Å; these distances are around 0.1–0.2 Å shorter compared to Ba1–As and Ba2–As distances (Table 6). Such "tighter" coordination could be attributed to the different environment and smaller coordination number. Assigning the residual peak to either Ga or As did not provide chemically sensible structural arrangements.

Although synchrotron X-ray powder diffraction patterns collected for polycrystalline $Ba_4Ga_5As_8$ agree satisfactorily with the patterns simulated from the single-crystal diffraction data, weak peaks remain unindexed, likely indicating the existence of a commensurate or incommensurate superstructure (see Figure S3 in the Supporting Information). This suggests that a threefold super-lattice [primitive monoclinic, a = 13.329(3) Å, b = 20.651(4) Å, c = 20.029(4) Å, β = 108.701(3)°] of the one indexed from the single-crystal data could exist. However, the in-house X-ray single-crystal diffractometer with a sealed Mo-K_α source (2 kW of power) could not provide the intensities to a sufficient $\sin\theta/\lambda$ resolution that would be needed to establish the superstructure.

EDX Analysis: Several $Ba_4Ga_5P_8$ and $Ba_4Ga_5As_8$ crystals from different reactions were subjected to elemental analysis by means of scanning electron microscopy/energy-dispersive using X-ray (SEM-EDX) analysis. This was done with the idea to independently confirm the compositions of these heavily disordered materials. The crystals were mounted onto a carbon tape and placed in a Jeol 7400 F electron microscope equipped with an INCA-Oxford energy-dispersive spectrometer. Multiple spots were analyzed for each crystal and then averaged. The determined compositions were consistent (within the error of the analysis) with the refined formulas.

Thermal Analysis: Differential scanning calorimetry thermogravimetric (DSC-TGA) analysis was carried out with a TA instrument model SDT Q600. Single crystals of each sample were selected under a microscope in the glovebox and ground into powder. The polycrystalline materials were transferred in alumina pans and loaded into the instrument. To prevent the samples from being oxidized at elevated temperature, a high purity argon flow (100 $cm^3 min^{-1}$) was used during the experiment. The samples were heated up at a rate of 10 $K min^{-1}$; different signals, including temperature, heat flow, and weight were recorded along the process. $CaGa_2P_2$ was found to decompose around 1323 K, concomitant to a significant weight loss (likely evaporation of P). The solid left in the alumina pan was checked by powder X-ray diffraction and found to be a mixture of Ga, GaP, and (an)other unidentified phase(s). $CaGa_2As_2$ showed similar thermal stability, whereas $SrGa_2As_2$ appeared to melt incongruently at approximately 1303 K. $Ba_2Ga_5As_5$ also melted incongruently near 1233 K. The recrystallization occurred at around the same temperature, and according to the powder diffraction patterns, one of the products was $Ba_4Ga_5As_8$. $Ba_4Ga_5P_8$ and $Ba_4Ga_5As_8$ appeared less thermally stable, both showing significant weight loss starting from around 1123 K.

Property Measurements: Needlelike crystals of $Ba_2Ga_5As_5$ were picked, and the Ga residual on the surface was mechanically removed under a microscope. Resistance was measured as a function of temperature (down to liquid He temperature) using the four-probe method.[52] Contacts were made with platinum wires using silver epoxy. A constant bias was applied to the outermost contacts while the current was measured through the innermost contacts. Resistivity was determined from the equation $\rho = RA/l$, for which A is the cross-section area of the crystal and l is the distance between the outermost contacts.

Seebeck coefficient measurements were measured in the temperature range of 100–300 K with a commercial MMR instrument installed with a K-20 programmable temperature controller and a SB-100 Seebeck controller. The two-contact setup allowed the measurements on $Ba_2Ga_5As_5$ and the smaller single crystals of $(Ba_{0.85(1)}Sr_{0.15})_2Ga_5As_5$. For $CaGa_2P_2$, the measurements were conducted on cold-pressed pellets.

Computational Methodology: Electronic structure calculations were performed with the aid of the Stuttgart TB-LMTO 4.7 program by employing the tight-binding linear muffin-tin orbital (TB-LMTO) method.[45,46] Exchange and correlation were treated with local density approximation (LDA).[53] All relativistic effects except for spin–orbital coupling were taken into account by the scalar relativistic approximation.[54] The basis set include 4s, 4p, and 3d orbitals for Ca; 5s, 5p, and 4d orbitals for Sr; 6s, 6p, 5d and 4f orbitals for Ba; 4s, 4p, and 4d orbitals for Ga; 4s, 4p, and 4d orbitals for As; and 3s, 3p, and 3d orbitals for P. The 4p orbital of Ca, 5p orbital of Sr, 6p orbital of Ba, 4d orbital of Ga, 4d orbital of As, and 3d

orbital of P were treated with the down-folding technique.[55] The *k*-space integrations were performed by the tetrahedron method.[56] The total and partial density of states (DOS) and crystal orbital Hamilton populations (COHP)[57] of selected interactions were plotted with the Fermi level set as a reference point at 0 eV.

Supporting Information (see footnote on the first page of this article): Tables with crystallographic information for $(Ba_{0.85(1)}Sr_{0.15})_2Ga_5As_5$, $Ba_4Ga_5P_8$ and $Ba_4Ga_5As_8$; description of the structural disorder and corresponding figures; synchrotron powder X-ray diffraction patterns for $Ba_4Ga_5As_8$; results from the EDX analysis on $Ba_4Ga_5As_8$; plot of the Seebeck coefficients (α) of $CaGa_2P_2$ as a function of the temperature; plot of the power factor ($\alpha^2\sigma$) of $Ba_2Ga_5As_5$ as a function of the temperature.

Acknowledgments

S. B. gratefully acknowledges funding from the University of Delaware and the Petroleum Research Fund (ACS-PRF). H. H. thanks the International Centre for Diffraction Data (ICDD) for a 2011 Ludo Frevel Fellowship. Use of the Advanced Photon Source was supported by the U. S. Department of Energy, Office of Science, Office of Basic Energy Sciences, under contract number DE-AC02-06CH11357.

[1] E. Zintl, *Angew. Chem.* **1939**, *52*, 1-6.
[2] a) H. Schäfer, B. Eisenmann, W. Müller, *Angew. Chem. Int. Ed. Engl.* **1973**, *12*, 694–712; b) H. G. von Schnering, *Nova Acta Leopold.* **1985**, *59*, 165–182.
[3] a) R. Nesper, *Prog. Solid State Chem.* **1990**, *20*, 1–45; b) S. M. Kauzlarich (Ed.), *Chemistry, Structure, and Bonding of Zintl Phases and Ions*, VCH, New York, **1996**.
[4] D. M. Rowe (Ed.), *CRC Handbook of Thermoelectrics*, CRC Press, New York, **1995**.
[5] S. M. Kauzlarich, S. R. Brown, G. J. Snyder, *Dalton Trans.* **2007**, 2099–2107.
[6] S. R. Brown, S. M. Kauzlarich, F. Gascoin, G. J. Snyder, *Chem. Mater.* **2006**, *18*, 1873–1877.
[7] F. Gascoin, S. Ottensmann, D. Stark, S. M. Haile, G. J. Snyder, *Adv. Funct. Mater.* **2005**, *15*, 1860–1864.
[8] I. Todorov, D. Y. Chung, L. Ye, A. J. Freeman, M. G. Kanatzidis, *Inorg. Chem.* **2009**, *48*, 4768–4776.
[9] a) H. Zhang, J.-T. Zhao, Y. Grin, X.-J. Wang, M.-B. Tang, Z.-Y. Man, H.-H. Chen, X.-X. Yang, *J. Chem. Phys.* **2008**, *129*, 164713; b) H. Zhang, M. Baitinger, M.-B. Tang, Z.-Y. Man, H.-H. Chen, X.-X. Yang, Y. Liu, L. Chen, Y. Grin, J.-T. Zhao, *Dalton Trans.* **2010**, *39*, 1101–1104.
[10] X.-J. Wang, M.-B. Tang, H.-H. Chen, X.-X. Yang, J.-T. Zhao, U. Burkhardt, Y. Grin, *Appl. Phys. Lett.* **2009**, *94*, 092106.
[11] S.-Q. Xia, S. Bobev, *J. Am. Chem. Soc.* **2007**, *129*, 4049–4057.
[12] B. Saparov, M. Saito, S. Bobev, *J. Solid State Chem.* **2011**, DOI:10.1016/j.jssc.2010.12.015.
[13] B. Saparov, S. Bobev, A. Ozbay, E. R. Nowak, *J. Solid State Chem.* **2008**, *184*, 432–440.
[14] S.-Q. Xia, S. Bobev, *Inorg. Chem.* **2006**, *45*, 7126–7132.
[15] S.-Q. Xia, S. Bobev, *J. Am. Chem. Soc.* **2007**, *129*, 10011–10018.
[16] B. Saparov, S.-Q. Xia, S. Bobev, *Inorg. Chem.* **2008**, *47*, 11237–11244.
[17] B. Saparov, H. He, X. H. Zhang, R. Greene, S. Bobev, *Dalton Trans.* **2010**, *39*, 1063–1070.
[18] P. C. Canfield, Z. Fisk, *Phil. Magn. B* **1992**, *65*, 1117.
[19] M. G. Kanatzidis, R. Pöttgen, W. Jeitschko, *Angew. Chem. Int. Ed.* **2005**, *44*, 6996–7023.
[20] G. S. Nolas, D. T. Morelli, T. M. Tritt, *Annu. Rev. Mater. Sci.* **1999**, *29*, 89–116.
[21] D. R. Lide (Ed.), *CRC Handbook of Chemistry and Physics*, 83rd ed., CRC Press, **2002–2003**.
[22] S.-Q. Xia, J. Hullmann, S. Bobev, *J. Solid State Chem.* **2008**, *181*, 1909–1914.
[23] S. Bobev, J. Hullmann, T. Harmening, R. Pöttgen, *Dalton Trans.* **2010**, *39*, 6049–6055.
[24] H. He, R. Stearrett, E. R. Nowak, S. Bobev, *Inorg. Chem.* **2010**, *49*, 7935–7940.
[25] S. J. Kim, M. G. Kanatzidis, *Inorg. Chem.* **2001**, *40*, 3781–3785.
[26] A. M. Goforth, H. Hope, C. L. Condron, S. M. Kauzlarich, N. Jensen, P. Klavins, S. MaQuilon, Z. Fisk, *Chem. Mater.* **2009**, *21*, 4480–4489.
[27] S. M. Park, S. J. Kim, M. G. Kanatzidis, *J. Solid State Chem.* **2003**, *175*, 310–315.
[28] J. Mathieu, R. Achey, J. H. Park, K. M. Purcell, S. W. Tozer, S. E. Latturner, *Chem. Mater.* **2008**, *20*, 5675–5681.
[29] J. Jiang, S. M. Kauzlarich, *Chem. Mater.* **2006**, *18*, 435–441.
[30] A. M. Goforth, P. Klavins, J. C. Fettinger, S. M. Kauzlarich, *Inorg. Chem.* **2008**, *47*, 11048–11056.
[31] J. F. Rauscher, C. L. Condron, T. Beault, S. M. Kauzlarich, N. Jensen, P. Klavins, S. MaQuilon, Z. Fisk, M. M. Olmstead, *Acta Crystallogr.* **2009**, *C65*, i69–i73.
[32] A. Bondi, *J. Phys. Chem.* **1964**, *68*, 441–451.
[33] G. Cordier, H. Ochmann, H. Schäfer, *Mater. Res. Bull.* **1986**, *21*, 331–336.
[34] L. Pauling, *The Nature of the Chemical Bond*, 3rd ed., Cornell University Press, Ithaca, NY, **1960**.
[35] S.-Q. Xia, S. Bobev, *Inorg. Chem.* **2008**, *47*, 1919–1921.
[36] The small difference in $d_{Ga–Ga}$ could be a "side effect" of the staggered conformation of Ga_2As_6 compared to the eclipsed conformation of Ga_2P_6.
[37] Taking into account the small disorder, the formula unit should be expressed as $Ba_{2+x}Ga_{5-2x}As_5$, that is, $Ba_{2.07(1)}Ga_{4.86(1)}As_5$ based on our refinement. The slight off-stoichiometry could explain the discrepancy between the theoretically predicted small band-gap semiconducting behavior (of $Ba_2Ga_5As_5$) and the metallic-like dependence of the electrical resistivity, determined for single crystals of $Ba_{2.07(1)}Ga_{4.86(1)}As_5$.
[38] P. Villars, L. D. Calvert, *Pearson's Handbook of Crystallographic Data for Intermetallic Phases*, 2nd ed., American Society for Metals, Materials Park, OH, **1991**.
[39] O. Seeger, J. Strähle, *Z. Naturforsch., Teil B* **1994**, *49*, 1169–1174.
[40] B. Eisenmann, H. Jordan, H. Schäfer, *Angew. Chem. Int. Ed. Engl.* **1981**, *20*, 197–198.
[41] P. Boher, P. Garnier, J. R. Gavarri, A. W. Hewat, *J. Solid State Chem.* **1985**, *57*, 343–350.
[42] B. Saparov, S. Bobev, *Inorg. Chem.* **2010**, *49*, 5173–5179.
[43] J. Peters, B. Krebs, *Acta Crystallogr., Sect. B* **1982**, *38*, 1270–1272.
[44] Refinements of the occupancy of Ga2, which describes the chains in the Ba_4GaP_4 slab in $Ba_4Ga_5P_8$, show that it is around 60% occupied, which means that in addition to isolated GaP_4 tetrahedra, there also are chainlike/oligomeric fragments. In $Ba_4Ga_5As_8$, which has a lower-symmetry structure, the isolated $GaAs_4$ tetrahedra are fully ordered, but electron density that remains between them and weak superstructure reflections in the synchrotron data (see Supporting Information) suggest the possible presence of longer units.
[45] a) O. K. Andersen, *Phys. Rev. B* **1975**, *12*, 3060–3083; b) O. K. Andersen, O. Jepsen, *Phys. Rev. Lett.* **1984**, *53*, 2571–2574; c) O. K. Andersen, Z. Pawlowska, O. Jepsen, *Phys. Rev. B* **1986**, *34*, 5253–5269; d) H. L. Skriver, *The LMTO Method*, Springer, Berlin, **1984**.
[46] O. Jepsen, O. K. Andersen, *The Stuttgart TB-LMTO Program, Version 4.7*, Max-Planck-Institut für Festkörperforschung, Stuttgart, Germany, **1998**.
[47] G. J. Miller, *Eur. J. Inorg. Chem.* **1998**, 523–536.
[48] a) A. C. Larson, R. B. Von Dreele, *General Structure Analysis System (GSAS)*, Los Alamos National Laboratory Report

LAUR 86-748, **1994**; b) B. H. Toby, *J. Appl. Crystallogr.* **2001**, *34*, 210–213.
[49] *Bruker SMART and SAINT*, Bruker AXS Inc., Madison, Wisconsin, USA., **2002**.
[50] G. M. Sheldrick, *SADABS*, University of Göttingen, Germany, **2003**.
[51] G. M. Sheldrick, *SHELXL*, University of Göttingen, Germany, **2001**.
[52] L. B. Valdes, *Proc. IRE* **1954**, *42*, 420–427.
[53] U. von Barth, L. Hedin, *J. Phys. C Solid State Phys.* **1972**, *5*, 1629–1642.
[54] D. D. Koelling, B. N. Harmon, *J. Phys. C: Solid State Phys.* **1977**, *10*, 3107–3114.
[55] W. R. L. Lambrecht, O. K. Andersen, *Phys. Rev. B: Condens. Matter* **1986**, *34*, 2439–2449.
[56] P. E. Blöchl, O. Jepsen, O. K. Andersen, *Phys. Rev. B: Condens. Matter* **1994**, *49*, 16223–16233.
[57] R. Dronskowski, P. E. Blöchl, *J. Phys. Chem.* **1993**, *97*, 8617–8624.

Received: January 19, 2011
Published Online: April 1, 2011

